IEEE Access
Multidisciplinary | Rapid Review | Open Access Journal

Received December 2, 2019, accepted December 16, 2019, date of publication January 3, 2020, date of current version January 28, 2020.

Digital Object Identifier 10.1109/ACCESS.2020.2963884

Two Separate Circles With Same-Radius: Projective Geometric Properties and Applicability in Camera Calibration

FENGLI YANG, YUE ZHAO, AND XUECHUN WANG
Institute of Mathematics and Statistics, Yunnan University, Kunming 650091, China

Corresponding author: Yue Zhao (zhao6685@yeah.net)

This work was supported in part by the National Natural Science Foundation of China (NSFC) under Grant 61663048 and Grant 11861075, in part by the Programme for Innovative Research Team (in Science and Technology) in Universities of Yunnan Province, and in part by the Key Joint Project of the Science and Technology Department of Yunnan Province and Yunnan University under Grant 2018FY001(-014).

ABSTRACT In the domain of computer vision, camera calibration is a key step in recovering the two-dimensional Euclidean structure. Circles are considered important image features similar to points, lines, and conics. In this paper, a novel linear calibration method is proposed using two separate same-radius (SSR) circles as the calibration pattern. We show that the distinct pair of dual circles encodes three lines, two of which are parallel to each other and perpendicular to the remaining line. When any two coplanar or parallel circles degenerate to SSR circles, a solution can be found to recover another pair of parallel lines based on the geometric properties of the SSR circles. Using the vanishing points obtained as the key helper for determining the imaged circular points and the orthogonal vanishing points, we deduce the constraints on the image of the absolute conic (IAC) and then employ it for complete camera calibration. Furthermore, a closed-form solution for the extrinsic parameters can be obtained based on the projective invariance of the conic dual to the circular points. Evaluations based on simulated and real data confirmed the effectiveness and feasibility of the proposed algorithms.

INDEX TERMS Camera calibration, conic dual, image of circular points, parallel lines, SSR circles.

I. INTRODUCTION

Camera calibration is an essential task in computer vision [1]–[3] because the intrinsic and extrinsic parameters of the camera are essential for three-dimensional (3D) reconstructions [4]–[6]. Given the rapid developments in modern vision applications, it has become important to develop simple and high-efficiency calibration algorithms for completing visual tasks. A number of calibration methods [7]–[9] have been proposed in recent years. Conventional self-calibration methods [10], [11] do not require any known space geometry; instead, they only need a certain number of matched image points between two or more images. However, these methods are sensitive to noise and do not yield accurate matching points. A sphere has isotropic visibility from any view [12], [13]. Hence, calibration technology using only a sphere as the pattern has been studied widely [14]–[16]. Huang *et al.* [17] explored a new linear calibration algorithm based on the properties of the common self-polar triangle of sphere images. They found that, for two separate sphere images, there exists a unique common self-polar triangle, which can be determined from the generalised eigenvectors of the two sphere images, with one of the vertices of the common self-polar triangle being an infinity point. Consequently, three sphere images can yield a vanishing line that can be used to calibrate the camera. Zhang *et al.* [18] established the relationship between the dual of the sphere image and the dual image of the absolute conic (DIAC). That is to say, the common pole-polar of the two sphere images is also the pole-polar with regards to the image of the absolute conic (IAC). Three sphere images can be used to completely calibrate the camera based on these algebraic constraints on the IAC. However, the size of the sphere, as well as the distance from the sphere projection to the principal point, may affect the calibration results. Recently, a conic, which is a common and simple two-dimensional (2D) object, was used

The associate editor coordinating the review of this manuscript and approving it for publication was Hugo Proenca.

in calibration, given that conics play an important role similar to points and lines and have more geometric information for camera calibration [19], [20]. Ying and Zha [21] considered two principal-axis-aligned (PAA) conics as the calibration pattern and showed that if the eccentricity of one of the PAA central conics is known, the two constraints on the IAC can be obtained from the image of the PAA. On the other hand, if the parameters of the PAA are not known, only one constraint on the IAC can be obtained. Based on the geometric properties of conics with a common axis of symmetry, Zhao [22] was able to obtain a solution for recovering the line at infinity and the symmetry axis, and also to deduce the constraints for determining the two-dimensional (2D) Euclidean structure. However, these special conics are difficult to obtain in practice.

In contrast, circles are available readily in daily life, and can also be extracted with precision from images, allowing for calibration with acceptable accuracy. Hence, circles [23]–[25] have been widely employed for camera calibration. For instance, Huang et al. [26] showed that there are an infinite number of common self-polar triangles for concentric circles; however, these common self-polar triangles share a common vertex, and their opposite side lies on the same line. An analysis of the algebraic properties of the common self-polar triangle indicates that the common vertex and its opposite side are the centre of the concentric circle and the infinite line on the supporting plane, respectively. Therefore, on the image plane, the image of the circle centre and the vanishing line can be determined by the generalised eigenvalue decomposition of the two concentric circles. Thus, the IAC can induce good constraints. Finally, the camera parameters can be extracted by decomposing the IAC. Chen and Wu [27] described a novel approach for recovering the common tangents of a circle-pair via the decomposition of degenerate conics. Moreover, the vanishing line of the supporting plane can be determined using two vanishing points in the image plane. Huang *et al.* [28] found that any two separating coplanar circles have a unique common self-polar triangle. Specifically, one vertex of the common self-polar triangle lies on the line at infinity. Given three separating circle images, the vanishing line of the support plane can be obtained, allowing the imaged circular points to be detected.

In this study, we employed two separate same-radius (SSR) circles as the calibration pattern. Employing a similar approach [29], Da *et al.* first obtained two pairs of conjugate complex intersections of two parallel circles. Next, the imaged circular points were recovered based on their quasi-affine invariance [30]. Owing to the tangent invariance of the perspective projection, the common tangents of two SSR circles and their intrinsic parameters were utilized to determine the extrinsic parameters. However, they did not provide a camera calibration method for estimating the intrinsic parameters. In addition, the equations for the computing extrinsic parameters are highly complex. Accordingly, in this study, we explored the geometric and algebraic properties of two SSR circles. We determined that two SSR circles encode three lines, two of which are parallel to each other and perpendicular to the remaining line. Based on the geometric properties of two SSR circles, it is possible to determine the line at infinity. Subsequently, the conic dual to the circular points can be recovered. Moreover, the planar homography and the IAC can be estimated correspondingly. In this study, we only used two SSR circles with unknown centres and radii. The novelty of the study is that it provides new insights about the geometric structures of two SSR circles based on the camera calibration problem.

The remainder of this paper is organised as follows. Section II briefly describes the projection model of the pinhole camera and the equation of the circle image. Section III describes in detail the calibration algorithms proposed based on the projective and geometric properties of two SSR circles. Section IV presents the results of simulations and compares them to those obtained using real data. Finally, Section V summarises the main findings of the study.

II. PRELIMINARIES

In this section, we briefly review the camera imaging model and the projection process of the circle.

A. MODEL OF PINHOLE CAMERA

In the world coordinate system $\mathbf{O}_w - X_wY_wZ_w$, there exists a space point $\mathbf{M} = \begin{bmatrix} X & Y & 0 & 1 \end{bmatrix}^{\mathrm{T}}$ on plane $\mathbf{O}_wX_wY_w$, such that the homogeneous coordinates of the corresponding point on the image plane after a projective transformation are $\mathbf{m} = \begin{bmatrix} x & y & 1 \end{bmatrix}^{\mathrm{T}}$. Hence, the relationship between them may be written in the matrix form as follows:

$$\lambda_m \mathbf{m} = \mathbf{K} \begin{bmatrix} \mathbf{R} & \mathbf{T} \end{bmatrix} \mathbf{M}, \tag{1}$$

where λ_m is a nonzero scale factor and $\begin{bmatrix} \mathbf{R} & \mathbf{T} \end{bmatrix}$ represents the extrinsic parameter matrix. The upper triangular matrix,

$$\mathbf{K} = \begin{bmatrix} f_u & s & u_0 \\ 0 & f_v & v_0 \\ 0 & 0 & 1 \end{bmatrix},$$

comprises the effective focal length f_u, f_v in terms of the pixel dimensions along the u, v-axes on the image plane, skew factor s, and principle point $\begin{bmatrix} u_0 & v_0 & 1 \end{bmatrix}^{\mathrm{T}}$.

Let the i^{th} $(i = 1, 2, 3)$ column of the rotation matrix, $\mathbf{R}$, be defined as $\mathbf{r}_i$. Then, (1) can be rewritten as follows:

$$\lambda_m \mathbf{m} = \mathbf{K} \begin{bmatrix} \mathbf{r}_1 & \mathbf{r}_2 & \mathbf{T} \end{bmatrix} \begin{bmatrix} X \\ Y \\ 1 \end{bmatrix}_i, \tag{2}$$

where $\mathbf{H} = \mathbf{K} \begin{bmatrix} \mathbf{r}_1 & \mathbf{r}_2 & \mathbf{T} \end{bmatrix}_i$ is the world-to-image homography [22].

B. EQUATION OF CIRCLE IMAGE

We consider two SSR circles on the world plane as the calibration target. Without loss of generality, the world coordinate system, $\mathbf{O}_w - X_wY_wZ_w$, is established on an arbitrary point in space with $\mathbf{O}_w$ as the origin (see Fig. 1),where the

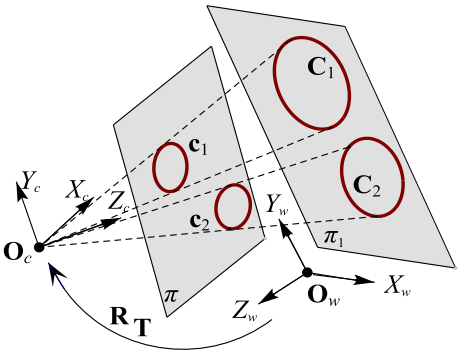

FIGURE 1. Projection model from world plane to image plane.

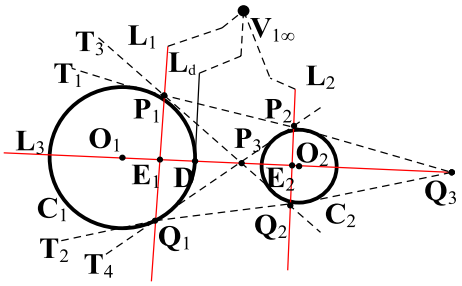

FIGURE 2. Properties of two coplanar or parallel circles: three lines can be obtained via generalised eigenvector decomposition, two of which are parallel to each other and perpendicular to the remaining line.

supporting plane of the two circles, $\mathbf{C}_1$ and $\mathbf{C}_2$, is the world plane, $\mathbf{O}_w X_w Y_w$. Fig. 1 also shows the camera coordinate system, $\mathbf{O}_c - X_c Y_c Z_c$, where another arbitrary point is set as the origin, $\mathbf{O}_c$; $\mathbf{R}$ and $\mathbf{T}$ are the rotation matrix and translation vector, respectively, between the world coordinate system and the camera coordinate system.

Given a point $\bar{\mathbf{M}} = \begin{bmatrix} X & Y & 1 \end{bmatrix}^{\mathrm{T}}$ on circle $\mathbf{C}_1$, the following relationship holds:

$$\bar{\mathbf{M}}^{\mathrm{T}} \mathbf{C}_1 \bar{\mathbf{M}} = 0. \tag{3}$$

Based on the above description, from (2), the image, $\mathbf{m}$, of $\bar{\mathbf{M}}$ should satisfy the following relationship:

$$\lambda_m \mathbf{m} = \mathbf{K} \begin{bmatrix} \mathbf{r}_1 & \mathbf{r}_2 & \mathbf{T} \end{bmatrix} \bar{\mathbf{M}} = \mathbf{H} \bar{\mathbf{M}}. \tag{4}$$

Based on Fig. 1, let conic $\mathbf{c}_1$ be the projection of $\mathbf{C}_1$ on the image plane, π, perpendicular to the Z_c-axis. According to the homogeneity of the projective transformation, image point $\mathbf{m}$ is on circle image $\mathbf{c}_1$, and the following relationship holds:

$$\mathbf{m}^{\mathrm{T}} \mathbf{c}_1 \mathbf{m} = 0. \tag{5}$$

As $\mathbf{H} = \mathbf{K} \begin{bmatrix} \mathbf{r}_1 & \mathbf{r}_2 & \mathbf{T} \end{bmatrix}$ is an invertible matrix, the substitution of (3) and (4) into (5) gives

$$\lambda_{c1} \mathbf{c}_1 = \mathbf{H}^{-\mathrm{T}} \mathbf{C}_1 \mathbf{H}^{-1}, \tag{6}$$

where λ_{c1} is a nonzero scale factor.

Similarly, if the conic $\mathbf{c}_2$ is the projection of the circle $\mathbf{C}_2$ on π, there is

$$\lambda_{c2} \mathbf{c}_2 = \mathbf{H}^{-\mathrm{T}} \mathbf{C}_2 \mathbf{H}^{-1}, \tag{7}$$

where λ_{c2} is a nonzero scale factor.

III. CALIBRATION METHOD

In this section, we discuss the properties of two coplanar or parallel circles and also show how to calibrate a camera linearly based on two SSR circles.

A. PROPERTIES OF TWO COPLANAR OR PARALLEL CIRCLES

Given two coplanar or parallel circles $\mathbf{C}_1$ and $\mathbf{C}_2$, we now introduce their envelopes $\mathbf{C}_1^*$ and $\mathbf{C}_2^*$, which span the linear family of circle envelopes, $\mathbf{C}^*(\beta)$ [19]. The family has the following form:

$$\mathbf{C}^*(\beta) = \mathbf{C}_1^* - \beta \mathbf{C}_2^*, \tag{8}$$

where $\beta \in \mathbb{C}$, and the circle envelopes $\mathbf{C}_1^*$ and $\mathbf{C}_2^*$ are the duals of the circle loci $\mathbf{C}_1$ and $\mathbf{C}_2$, respectively [31]. When $\mathbf{C}_1$ and $\mathbf{C}_2$ are invertible matrices, $\mathbf{C}_1^* \propto \mathbf{C}_1^{-1}$, $\mathbf{C}_2^* \propto \mathbf{C}_2^{-1}$, where $\propto$ indicates equality up to a nonzero scale factor.

Consider the pencil of two dual (or line) conics, $\mathbf{C}_1^*$ and $\mathbf{C}_2^*$. Then, $\mathbf{C}_1^* - \lambda \mathbf{C}_2^*$ represents a conic that passes through all the common tangents of $\mathbf{C}_1^*$ and $\mathbf{C}_2^*$ [32]. Therefore, the conic family $\mathbf{C}^*(\beta)$ includes three members called degenerate conics, which consist of point-pairs corresponding to the generalised eigenvalues of $\left(\mathbf{C}_1^*, \mathbf{C}_2^*\right)$ [22].

As shown in Fig. 2, all envelopes of conic family $\mathbf{C}^*(\beta)$ touch the four real tangents that are common to two dual conic $\mathbf{C}_1^*$ and $\mathbf{C}_2^*$. Further, the degenerate members are the pairs of the common points on the common tangent-pairs, namely, $(\mathbf{P}_1, \mathbf{Q}_1)$, $(\mathbf{P}_2, \mathbf{Q}_2)$, and $(\mathbf{P}_3, \mathbf{Q}_3)$, which satisfy the following relationship:

$$\mathbf{C}_1^* - \beta \mathbf{C}_2^* = \mathbf{P}\mathbf{Q}^{\mathrm{T}} + \mathbf{Q}\mathbf{P}^{\mathrm{T}}, \tag{9}$$

where β is the generalised eigenvalue of $\left(\mathbf{C}_1^*, \mathbf{C}_2^*\right)$, which can be determined by solving

$$\left|\mathbf{C}_1^* - \beta \mathbf{C}_2^*\right| = 0. \tag{10}$$

Proposition 1: In Fig. 2, assuming that $\mathbf{C}_1$ *and* $\mathbf{C}_2$ *are two coplanar or parallel circles, the dual circle-pair* $\left(\mathbf{C}_1^*, \mathbf{C}_2^*\right)$ *encodes three lines* $\mathbf{L}_i (i = 1, 2, 3)$*, which consist of degenerate members* $(\mathbf{P}_i, \mathbf{Q}_i)$ *of the circle pencil* $\mathbf{C}^*(\beta)$ *and represent three sides of the common self-polar triangle of circles* $\mathbf{C}_1$ *and* $\mathbf{C}_2$*, such that* $\mathbf{L}_1$ *and* $\mathbf{L}_2$ *are parallel and perpendicular to the other line,* $\mathbf{L}_3$*.*

The proof of Proposition 1 is given in Appendix A.

B. TWO LINEAR CALIBRATION THEORIES BASED ON TWO SSR CIRCLES

Based on the algebraic and geometric properties of the circle family, it is easy to prove the following proposition:

Proposition 2: From images $\mathbf{c}_1$ *and* $\mathbf{c}_2$ *of two SSR circles, vanishing line* $\mathbf{l}_\infty$ *can be obtained via generalised eigenvalue decomposition.*

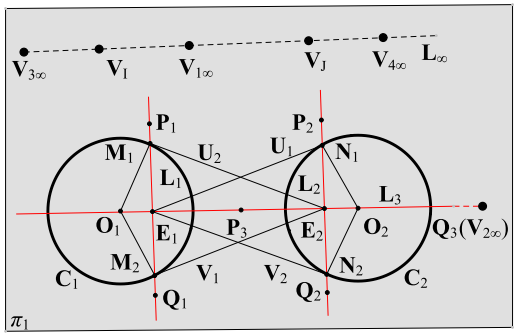

FIGURE 3. Recovery of parallel lines from model based on SSR circles.

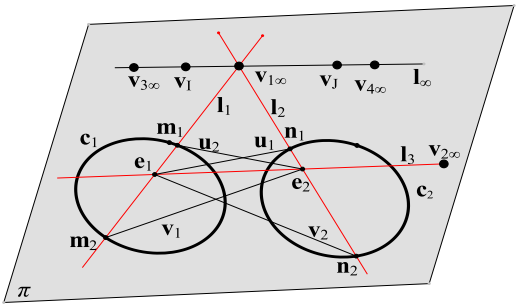

FIGURE 4. Schematic diagram of vanishing line.

The proof of Proposition 2 is shown in Appendix B.

Proposition 3: There exist the images, $\mathbf{c}_1$ *and* $\mathbf{c}_2$*, of the two SSR circles on the image plane,* π*. Then, the imaged circular points,* $\mathbf{v}_\mathrm{I}$ *and* v_J*, can be obtained.*

Proof: Based on Proposition 2, we can obtain the vanishing line, $\mathbf{l}_\infty$, once the images, $\mathbf{c}_1$ and $\mathbf{c}_2$, of the two SSR circles have been identified. This is because the vanishing line, $\mathbf{l}_\infty$, is the projection of the infinity line, $\mathbf{L}_\infty$, on plane π_1, and any circle will intersect $\mathbf{L}_\infty$ at the circular points, $\mathbf{V}_\mathrm{I}n$ and $\mathbf{V}_\mathrm{J}$.

As shown in Fig. 4, the vanishing line, $\mathbf{l}_\infty$, intersects circle image $\mathbf{c}_1$ at the imaged circular points, $\mathbf{v}_\mathrm{I}$ and $\mathbf{v}_\mathrm{J}$. Thus, the following two equations can be obtained:

$$\begin{cases} \mathbf{v}_{1\mathrm{I}}^{\mathrm{T}}\,\mathbf{c}_1\mathbf{v}_{1\mathrm{I}} = 0 \\ \mathbf{v}_{1\mathrm{I}}^{\mathrm{T}}\,\mathbf{l}_\infty = 0, \end{cases} \tag{11}$$

$$\begin{cases} \mathbf{v}_{1\mathrm{J}}^{\mathrm{T}}\,\mathbf{c}_1\mathbf{v}_{1\mathrm{J}} = 0 \\ \mathbf{v}_{1\mathrm{J}}^{\mathrm{T}}\,\mathbf{l}_\infty = 0. \end{cases} \tag{12}$$

Similarly, imaged circular points $\mathbf{v}_\mathrm{I}$ and $\mathbf{v}_\mathrm{J}$ also lie on circle image $\mathbf{c}_2$. Thus, two other equations can be obtained, as follows:

$$\begin{cases} \mathbf{v}_{2\mathrm{I}}^{\mathrm{T}}\,\mathbf{c}_2\mathbf{v}_{2\mathrm{I}} = 0, \\ \mathbf{v}_{2\mathrm{I}}^{\mathrm{T}}\,\mathbf{l}_\infty = 0 \end{cases} \tag{13}$$

$$\begin{cases} \mathbf{v}_{2\mathrm{J}}^{\mathrm{T}}\,\mathbf{c}_2\mathbf{v}_{2\mathrm{J}} = 0. \\ \mathbf{v}_{2\mathrm{J}}^{\mathrm{T}}\,\mathbf{l}_\infty = 0 \end{cases} \tag{14}$$

Theoretically, the same solutions to $\mathbf{v}_\mathrm{I}$ and $\mathbf{v}_\mathrm{J}$ are obtained from (11), (12), (13), and (14); however, they may differ because of noise. Therefore, to obtain accurate results, we take the average values of the solutions as the imaged circular points, $\mathbf{v}_\mathrm{I}$ and $\mathbf{v}_\mathrm{J}$:

$$\begin{cases} \mathbf{v}_I = (\mathbf{v}_{1\mathrm{I}} + \mathbf{v}_{2\mathrm{I}})/2. \\ \mathbf{v}_\mathrm{J} = (\mathbf{v}_{1\mathrm{J}} + \mathbf{v}_{2\mathrm{J}})/2 \end{cases} \tag{15}$$

□

Proposition 4: When the images of the two SSR circles, $\mathbf{c}_1$ *and* $\mathbf{c}_2$*, are known, a set of orthogonal vanishing points* $(\mathbf{v}_{1\infty}, \mathbf{v}_{2\infty})$ *can be obtained.*

Proof: As shown in Fig. 3, because the direction of lines $\mathbf{L}_1$ and $\mathbf{L}_2$ is orthogonal to the direction of line $\mathbf{L}_3$, the infinity point, $\mathbf{V}_{1\infty}$, on $\mathbf{L}_1$ and $\mathbf{L}_2$ and the infinity point, $\mathbf{V}_{2\infty}$, on $\mathbf{L}_3$ constitute a set of orthogonal infinity points. According to projective invariance, two lines, $\mathbf{l}_1$ and $\mathbf{l}_2$, intersect at vanishing point $\mathbf{v}_{1\infty}$ (see Fig. 4). Vanishing point $\mathbf{v}_{2\infty}$ can be determined based on the intersection of vanishing lines $\mathbf{l}_\infty$ and $\mathbf{l}_3$:

$$\lambda_{v2}\mathbf{v}_{2\infty} = \mathbf{l}_\infty \times \mathbf{l}_3, \tag{16}$$

where λ_{v2} is a nonzero scale factor. □

C. DETERMINING EXTRINSIC PARAMETERS

In the Euclidean coordinate system, conic $\mathbf{C}_\infty^*$ is a degenerate (rank 2) line conic, which consists of the two circular points [31]. It is given in matrix form by

$$\mathbf{C}_\infty^* = \mathbf{V}_\mathrm{I}\mathbf{V}_\mathrm{J}^{\mathrm{T}} + \mathbf{V}_\mathrm{J}\mathbf{V}_\mathrm{I}^{\mathrm{T}} = \begin{bmatrix} 1 & 0 & 0 \\ 0 & 1 & 0 \\ 0 & 0 & 0 \end{bmatrix}. \tag{17}$$

For circles, $\mathbf{C}_\infty^*$ is fixed not only under the scale and translation transformations but also under the rotation transformation [21].

Based on the definition of the dual conic $\mathbf{C}_\infty^*$, we get the following three properties of $\mathbf{C}_\infty^*$ in any projective frame:

Property 1 [31]: $\mathbf{C}_\infty^*$ *has four degrees of freedom: a* 3×3 *homogeneous symmetric matrix has five degrees of freedom; however, the constraint* $\det \mathbf{C}_\infty^* = 0$ *reduces the degrees of freedom by one.*

Property 2 [31]: $\mathbf{L}_\infty$ *is the null vector of* $\mathbf{C}_\infty^*$*. Because the circular points are a pair of complex conjugate points,* $\mathbf{v}_\mathrm{I}^{\mathrm{T}}\mathbf{L}_\infty = \mathbf{v}_\mathrm{J}^{\mathrm{T}}\mathbf{L}_\infty = 0$*. Then,*

$$\mathbf{C}_\infty^*\mathbf{L}_\infty = \left(\mathbf{V}_\mathrm{I}\mathbf{V}_\mathrm{J}^{\mathrm{T}} + \mathbf{V}_\mathrm{J}\mathbf{V}_\mathrm{I}^{\mathrm{T}}\right)\mathbf{L}_\infty = 0 \tag{18}$$

Property 3 [31]: Perpendicular lines $\mathbf{L}_1$ *and* $\mathbf{L}_3$ *are conjugate with respect to* $\mathbf{V}_\mathrm{I}\mathbf{V}_\mathrm{J}$ *and satisfy the following condition:*

$$\mathbf{L}_1^{\mathrm{T}}\mathbf{C}_\infty^*\mathbf{L}_3 = 0. \tag{19}$$

Proposition 5: The images of the two SSR circles, $\mathbf{c}_1$ *and* $\mathbf{c}_2$*, provide enough constraints to compute the image,* $\mathbf{c}_\infty^*$*, of the conic dual to the circular points.*

Proof: Given the images of the two SSR circles, $\mathbf{c}_1$ and $\mathbf{c}_2$, vanishing line $\mathbf{l}_\infty$ can be obtained from Proposition 2. Further, the two lines, $\mathbf{l}_1$ and $\mathbf{l}_3$, that are the projections of perpendicular lines $\mathbf{L}_1$ and $\mathbf{L}_3$, can also be computed from

the generalised eigenvalue decomposition. Therefore, there are enough constraints for estimating the image of $\mathbf{C}^*_\infty$:

$$\begin{cases} \mathbf{c}^*_\infty \mathbf{l}_\infty = 0. \\ \mathbf{l}_1^{\mathrm{T}} \mathbf{c}^*_\infty \mathbf{l}_3 = 0 \end{cases} \tag{20}$$

□

Proposition 6: Once conic $\mathbf{c}^*_\infty$ has been identified on the projective plane, the extrinsic parameters of the camera can be determined.

Proof: Under the point transformation $\mathbf{m} = \mathbf{HM}$, where $\mathbf{H} = \mathbf{K}\begin{bmatrix}\mathbf{r}_1 & \mathbf{r}_2 & \mathbf{T}\end{bmatrix}$ is world-to-image homography, conic $\mathbf{C}^*_\infty$ transforms to $\mathbf{c}^*_\infty = \mathbf{H}\mathbf{C}^*_\infty\mathbf{H}^{\mathrm{T}}$. Actually, $\mathbf{c}^*_\infty$ identified in an image plane using the SVD decomposition can be written as follows:

$$\mathbf{c}^*_\infty = \mathbf{U}\begin{bmatrix} 1 & 0 & 0 \\ 0 & 1 & 0 \\ 0 & 0 & 0 \end{bmatrix}. \tag{21}$$

The homography is $\mathbf{H} = \mathbf{U}$ up to a scale and translation transformation. From (2), we have the following:

$$\lambda_h \mathbf{K}^{-1}\mathbf{H} = \begin{bmatrix}\mathbf{r}_1 & \mathbf{r}_2 & \mathbf{T}\end{bmatrix}. \tag{22}$$

Because rotation matrix $\mathbf{R}$ is an orthogonal matrix, the scale factor, λ_h, can be determined. Then, from (22), we have

$$\begin{cases} \mathbf{r}_1 = \lambda_h \mathbf{K}^{-1}\mathbf{h}_1 \\ \mathbf{r}_2 = \lambda_h \mathbf{K}^{-1}\mathbf{h}_2, \\ \mathbf{r}_3 = \mathbf{r}_1 \times \mathbf{r}_2 \\ \mathbf{T} = \lambda_h \mathbf{K}^{-1}\mathbf{h}_3 \end{cases} \tag{23}$$

where $\mathbf{h}_i (i = 1, 2, 3)$ is the i^{th} column of $\mathbf{H}$. Therefore, after calibrating the camera using the images of two SSR circles, extrinsic parameters $\begin{bmatrix}\mathbf{R} & \mathbf{T}\end{bmatrix}$ can be derived from homography $\mathbf{H}$. □

D. ALGORITHM

In projective geometry, the two special points (the circular points) on the infinity line play a vital role and have the canonical forms $\mathbf{V}_{\mathrm{I}} = \begin{bmatrix}1 & i & 0\end{bmatrix}^{\mathrm{T}}$ and $\mathbf{V}_{\mathrm{J}} = \begin{bmatrix}1 & -i & 0\end{bmatrix}^{\mathrm{T}}$. Obviously, both $\mathbf{V}_{\mathrm{I}}$ and $\mathbf{V}_{\mathrm{J}}$ satisfy the following conditions: $\mathbf{V}_{\mathrm{I}}^{\mathrm{T}}\mathbf{V}_{\mathrm{I}} = 0$, $\mathbf{V}_{\mathrm{J}}^{\mathrm{T}}\mathbf{V}_{\mathrm{J}} = 0$. Hence, $\mathbf{V}_{\mathrm{I}}$ and $\mathbf{V}_{\mathrm{J}}$ also lie on the absolute conic (AC). If the imaged circular points are denoted by $\mathbf{v}_{\mathrm{I}}$ and $\mathbf{v}_{\mathrm{J}}$, then the following relationships are satisfied:

$$\mathbf{v}_{\mathrm{I}}^{\mathrm{T}}\boldsymbol{\omega}\mathbf{v}_{\mathrm{I}} = 0, \tag{24}$$

and

$$\mathbf{v}_{\mathrm{J}}^{\mathrm{T}}\boldsymbol{\omega}\mathbf{v}_{\mathrm{J}} = 0, \tag{25}$$

where $\boldsymbol{\omega}$ is the matrix form of the IAC. Because $\boldsymbol{\omega}$ is a 3×3 symmetric matrix with five degrees of freedom, and the imaged circular points, $\mathbf{v}_{\mathrm{I}}$ and $\mathbf{v}_{\mathrm{J}}$, are a pair of complex conjugate points, only the real and imaginary parts of $\mathbf{v}_{\mathrm{I}}$ or $\mathbf{v}_{\mathrm{J}}$ separately can provide a constraint. Hence, we need at least three pairs of circular points for determining the IAC.

Let us assume a pair of vanishing points, $\mathbf{v}_{1\infty}$ and $\mathbf{v}_{2\infty}$, from two orthogonal sets of space parallel lines. Then, points $\mathbf{v}_{1\infty}$ and $\mathbf{v}_{2\infty}$ are conjugate with respect to the IAC [31]. In other words,

$$\mathbf{v}_{1\infty}^{\mathrm{T}}\boldsymbol{\omega}\mathbf{v}_{2\infty} = 0. \tag{26}$$

Because $\boldsymbol{\omega}$ only has five degrees of freedom, it can be estimated if at least five pairs of orthogonal vanishing points are known. However, in general, for all the orthogonal vanishing points on a plane, only two sets of orthogonal vanishing points are linearly independent [31]. Hence, there are at least three sphere images for estimating $\boldsymbol{\omega}$.

Based on the above discussion, the proposed camera calibration algorithms can be summarized as follows:

Step 1. Take $n\,(n \geq 3)$ images of two SSR circles at different orientations, and extract the pixel coordinates of two conics on each image. Next, fit the coefficients of the two conics, $\mathbf{c}_{nj}$ $(j = 1, 2)$, using the least squares method [35].

Step 2. Using (27), compute the generalised eigenvectors $\mathbf{l}_{ni}$ of the conic-pairs, $(\mathbf{c}_{n1}, \mathbf{c}_{n2})$, on each image.

Step 3. Determine line $\mathbf{l}_{n3}$ from the generalised eigenvectors; this is the only line having two intersection points with both $\mathbf{c}_{n1}$ and $\mathbf{c}_{n2}$. Furthermore, the vanishing points, $\mathbf{v}_{n1\infty}$, $\mathbf{v}_{n3\infty}$, and $\mathbf{v}_{n4\infty}$, on the world plane, π_{n1}, can be obtained using Proposition 2.

Step 4. Obtain vanishing line $\mathbf{l}_{n\infty}$ on plane π_{n1} using (41). Further, estimate the images of the circular points, $\mathbf{v}_{n\mathrm{I}}$ and $\mathbf{v}_{n\mathrm{J}}$, on the conics, $\mathbf{c}_{n1}$ and $\mathbf{c}_{n2}$, from (11)−(15). Next, compute the two pairs of orthogonal vanishing points, $\mathbf{v}_{n1\infty}$ and $\mathbf{v}_{n2\infty}$, based on the pole-polar relationship.

Step 5. Determine the IAC, $\boldsymbol{\omega}$, from the constraint equation, that is, (24) or (26), of the IAC and then determine the intrinsic parameters $\mathbf{K}$ by Cholesky factorization and matrix inversion for $\boldsymbol{\omega}$.

Step 6. Determine the extrinsic parameters of the camera, $\mathbf{R}_n$ and $\mathbf{T}_n$, as described in Section III.C.

IV. EXPERIMENTS

We performed a number of experiments using both simulated data and real images to evaluate the proposed methods. During the simulations, the sensitivity of the algorithms to noise was tested. On the other hand, during the experiments performed using real images, the camera pose was estimated based on the obtained intrinsic parameters. In addition, the 3D reconstruction results were analysed. In general, the imaged circular points and orthogonal vanishing points are harmonic conjugate [31]. However, in the experiments, we considered which method to use based on the test performance, namely, to determine whether the image of the absolute conic is positive definite. The proposed algorithms were compared with other algorithms to evaluate their effectiveness and feasibility. The calibration algorithms based on the images of the circular points and the orthogonal vanishing points are denoted as ICP and OVP, respectively. A previously reported algorithm [28] that uses the common self-polar triangle of separate circles is denoted as CST, while an algorithm [29] based on two similar circles is denoted as TSC. Finally, an algorithm [27] that uses circle-pairs with common tangents is denoted as CCT.

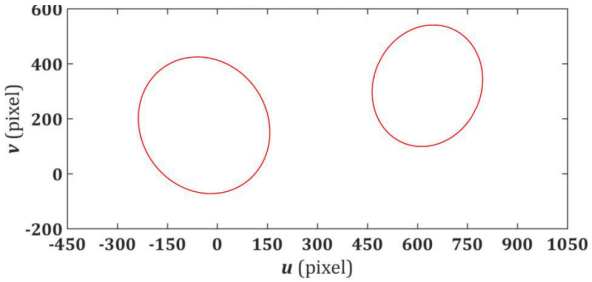

FIGURE 5. Images of two SSR circles generated using simulated camera.

TABLE 1. Mean values and percentage errors of intrinsic parameters determined based on synthetic data.

Calibration Methods	Parameters				
	$f_u(\%)$	$f_v(\%)$	$s(\%)$	$u_0(\%)$	$v_0(\%)$
Ground Truth	800	880	0.2	320	240
ICP	810.68	895.06	0.22	314.22	244.16
	(1.34)	(1.71)	(10.00)	(1.81)	(1.73)
OVP	813.31	898.24	0.24	312.15	234.24
	(1.66)	(2.07)	(20.00)	(2.45)	(2.40)
CST	792.29	891.87	0.21	323.67	236.92
	(0.96)	(1.35)	(5.00)	(1.15)	(1.28)
TSC	816.13	858.91	0.27	328.86	245.51
	(2.02)	(2.40)	(35.00)	(2.77)	(2.30)
CCT	788.87	863.62	0.22	326.34	235.32
	(1.39)	(1.86)	(10.00)	(1.98)	(1.95)

A. SIMULATIONS

Let the initial intrinsic matrix of the simulated camera be

$$\mathbf{K} = \begin{bmatrix} 800 & 0.2 & 320 \\ 0 & 880 & 240 \\ 0 & 0 & 1 \end{bmatrix}.$$

According to the proposed calibration algorithms, three images of two SSR circles are enough for fully calibrating the camera. Hence, we simulated three images of two SSR circles, one of which is shown in Fig. 5.

In the case of each image, the Canny edge detection operator [36] was used to extract 200 data points on the conic image of the two SSR circles. Next, the conic coefficients were determined using the least squares method. Furthermore, we performed 500 independent experiments and determined the average values and percentage errors of the intrinsic parameters recovered using the five approaches; the values are listed in Table 1. It can be seen from the results that ICP performed better than TSC and CCT in estimating the intrinsic parameters; however, its accuracy was slightly lower than that of CST.

Moreover, the performance of ICP as well as those of CST, TSC, and CCT were analysed in the presence of noise. For this, 200 pixel points on each circle image were corrupted with zero-mean Gaussian noise with different square deviations, σ (ranging from zero to three pixels). The noisy points were then fitted to obtain the circle images. For each noise level (σ), we performed 500 independent trials using the five algorithms and computed the mean values of the intrinsic parameters over each run, as shown in Figs. 6(a)–(e). The accuracy of estimating the intrinsic parameters decreased with the increase in the noise level, σ. However, the decreases in the case of ICP, OVP, CST, and CCT were similar; this may be owing to the fact that the four algorithms are linear calibration algorithms with stronger antinoise characteristics, whereas TSC is a nonlinear algorithm. In addition, CST exhibited higher precision than ICP and OVP, because it uses three circles, which can provide more constraints. However, for the same noise level, ICP performed better than CCT owing to the existence of a few degenerate cases when the input was not restricted. Therefore, it was confirmed that ICP and OVP are both feasible and effective.

TABLE 2. Runtimes (in seconds) of five algorithms (ICP, OVP, CST, TSC, AND CCT).

	Calibration Methods				
	ICP	OVP	CST	TSC	CCT
Runtime	0.15	0.21	0.13	0.88	0.57

The runtime for each method was calculated using MATLAB (R2016b) on a 2.1 GHz Intel Core i3 processor. The comparison results are presented in Table 2. It can be seen from the table that the runtime of TSC was approximately six times longer than that of ICP, possibly because TSC is a nonlinear approach and involves solving a quadratic polynomial equation. Further, the runtime of CCT was approximately four times longer than that of ICP because it involves the decomposition of the degenerate conic. In addition, ICP was slightly faster than OVP.

B. EXPERIMENTS USING REAL IMAGES

We also performed evaluations using actual images to fully evaluate the proposed calibration algorithm. For this, we used a test pattern consisting of two circles, both with a radius of 45 mm, as shown in Fig. 7. Because CST requires three separate circles for camera calibration, we did not use CST in these tests. All the real images used were taken with an industrial camera with an effective focal length of 16 mm. Further, the clear image range was 250–350 mm, and the image resolution was 1132×1029 pixels. In general, Zhang's approach [37] is used extensively owing to its high accuracy and robustness. Therefore, using Zhang's results as the true values, the calibration errors of the four algorithms were analysed. During the evaluation tests, a planar chessboard with 9×9 feature points was used to calibrate the camera; the horizontal and vertical spacing between any two adjacent feature points was 24 mm, and the target accuracy was 0.1 mm.

First, the Canny operator [36] was employed to detect the edges of the circle images, as shown in Fig. 8; this was done using the MATLAB toolbox. Moreover, the conics were obtained using a least squares ellipse fitting algorithm. In particular, there may be a case in which a circle wholly or partially covers another when the camera is in a critical position. For the contour with partial occlusion, a fast

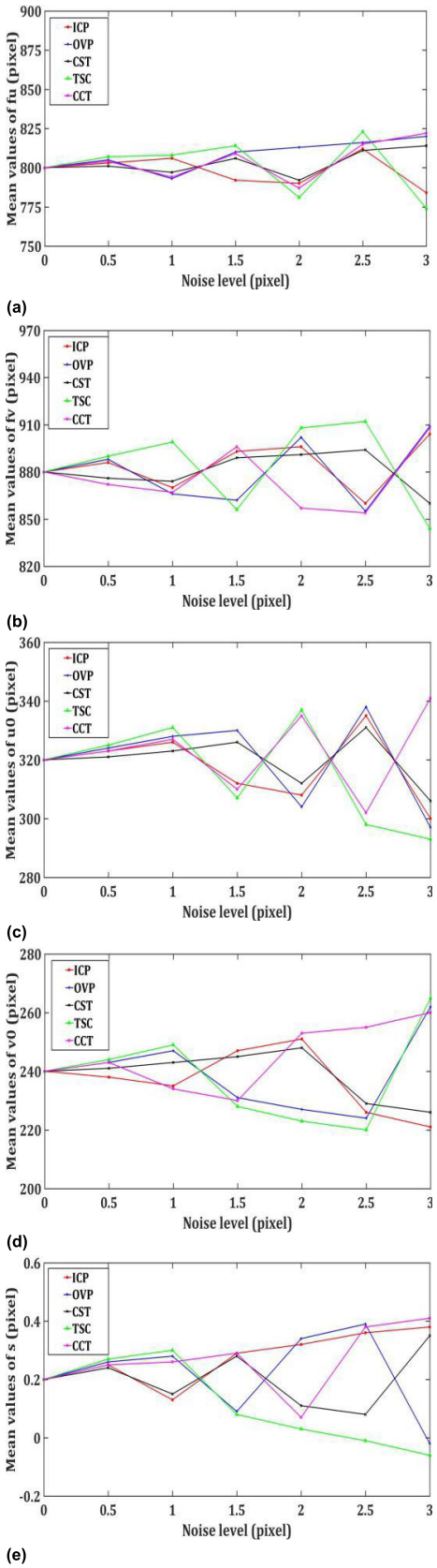

FIGURE 6. Comparison of sensitivities of five calibration algorithms for different noise levels. Average values of f_u, f_v, u_0, v_0, s are plotted in (a), (b), (c), (d), and (e), respectively.

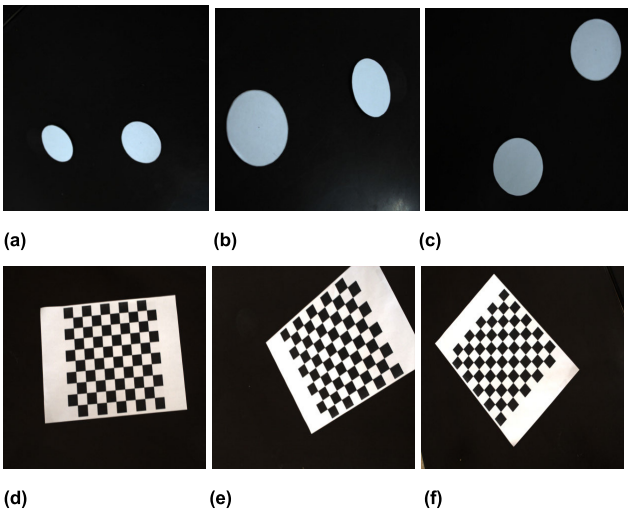

FIGURE 7. Three images of (a), (b), (c) two SSR circles and (d), (e), (f) chessboard obtained using digital camera.

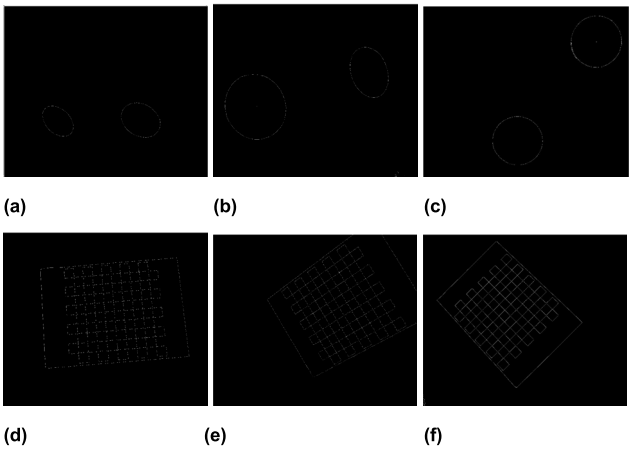

FIGURE 8. (a)-(f) Edge detection of three circle images and three chessboard images using Canny operator.

and effective method [15] was adopted to detect the circle images automatically.

To ensure more stable and robust results, we used the four algorithms to perform 100 independent tests and took the average values as the final calibration results, which are listed in Table 3. It can be seen from the table that the calibration results for the four algorithms were similar and close to those for Zhang's method. Moreover, the values of the angle between the abscissa and ordinate of the image coordinate system, $\theta = a\tan(f_u/abs(s))$ [31], as determined by ICP and OVP were 89.9991° and 89.9940°, respectively, whereas that for Zhang's method is 89.9977°. These values are very close to the ideal angle of 90.0000°. This confirmed that the proposed algorithms are effective and feasible within a certain error range.

In addition, we explored the effect of changes in the radius of the circles on the calibration accuracy. First, we used ICP

TABLE 3. Results of calibration using actual images.

Parameters	Calibration Methods				
	ICP	OVP	TSC	CCT	Zhang's
f_u	1662.18	1663.65	1664.28	1662.94	1660.84
f_v	1661.09	1660.54	1660.10	1662.53	1659.82
s	1.35	1.50	1.55	1.47	1.39
u_0	1125.91	1126.35	1127.36	1126.64	1124.26
v_0	1137.51	1139.04	1130.57	1138.14	1135.17
α	82.42	83.14	85.21	—	83.21
β	-23.24	-24.32	-26.11	—	-23.02
γ	15.54	16.33	18.04	—	14.81
$\mathbf{T}$	$\begin{bmatrix} 0.54 \\ -0.31 \\ 0.87 \end{bmatrix}$	$\begin{bmatrix} 0.77 \\ -0.35 \\ 0.86 \end{bmatrix}$	$\begin{bmatrix} 0.61 \\ -0.33 \\ 0.88 \end{bmatrix}$	—	$\begin{bmatrix} 1.42 \\ 3.58 \\ 0.87 \end{bmatrix}$

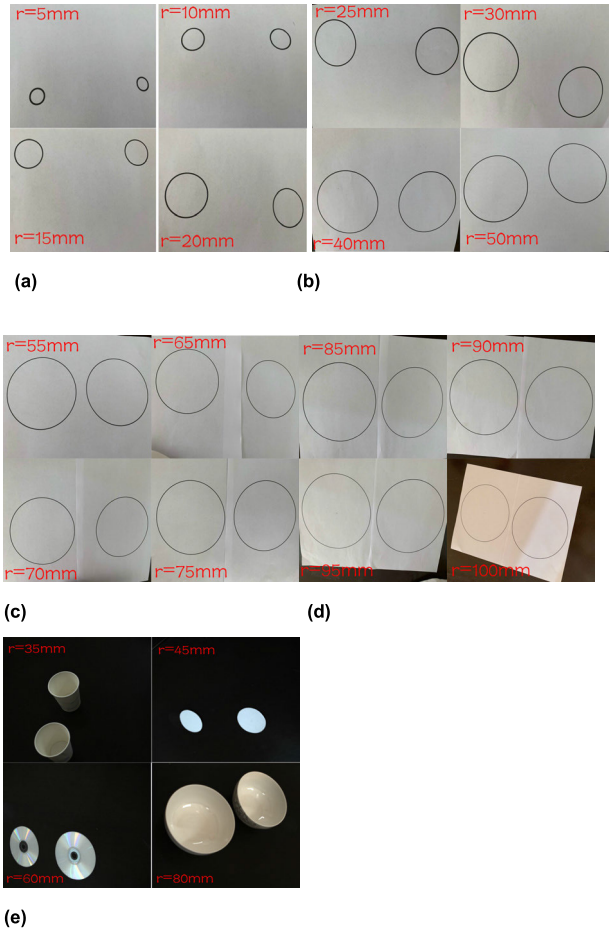

FIGURE 9. Image of SSR circles with different radii: (a), (b), (c), (d) artificial circular targets, and (e) common circles.

and OVP with two SSR circles with different radii varying from 5 to 100 mm; thereinto, to clarify the practicability of the proposed approach, four common circles (cups, covers, CDs and bowls) were taken by the digital camera, as shown in Figs. 9 and 10. Then, for each radius, we performed

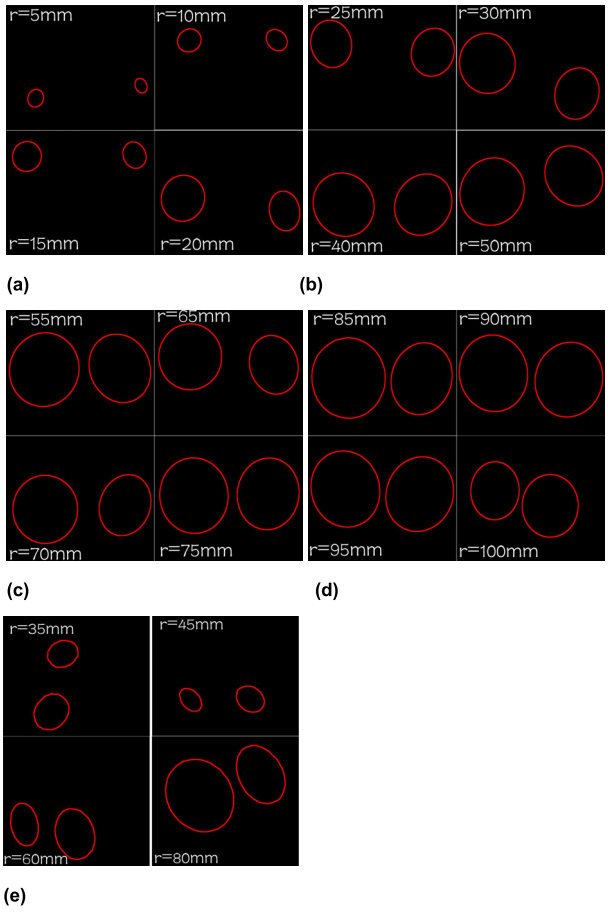

FIGURE 10. Edge detection of different SSR circles using Canny operator: (a), (b), (c), (d) artificial circular targets, and (e) common circles.

500 independent trials and computed the average relative error between the calculated intrinsic parameters and their true values. As the performances for f_u and f_v, u_0, and v_0 are similar, we show the data for f_u, u_0, and s, as shown in Fig. 11. It can be seen from the figure that the relative errors of the intrinsic parameters decreased significantly with the increase in the radius of the circles. It is possible that the larger the radius of the circle in the fixed position, the larger the projection is. Hence, more contour points can be obtained, resulting in a more accurate conic fitting.

For further comparison, we first extracted the angular points of the chessboard in Fig 8. In addition, based on the epipolar geometric constraints [38], 3D reconstruction was performed using the camera parameters listed in Table 3; the results are shown in Fig. 12.

Furthermore, we analysed the relative positioning error [39] between the reconstructed angular points. In the case of the world coordinate system, the relative positioning error refers to the error between the distances of every two neighbour reconstructed points and that of the actual target angular points. For each method, we performed 100 independent trials, and computed the mean values of the relative positioning errors over each run. The results are

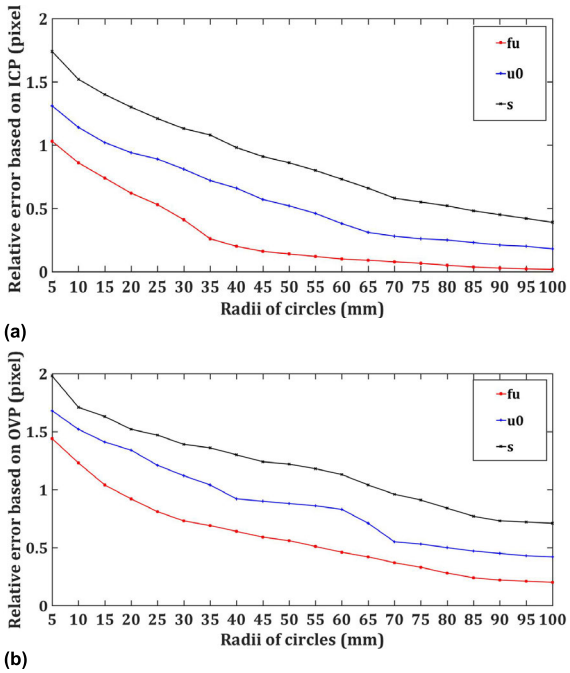

FIGURE 11. Relative error of recovered parameters for different circle radii: (a) ICP and (b) OVP.

TABLE 4. Mean values of relative positioning errors in horizontal and vertical directions (mm).

	Calibration Methods				
	ICP	OVP	TSC	CCT	Zhang's
Horizontal	0.78	0.94	1.31	0.84	0.34
Vertical	0.75	0.96	1.24	0.84	0.32

TABLE 5. Average angle (degree) of any two lines in parallel and orthogonal directions.

	Calibration Methods				
	ICP	OVP	TSC	CCT	Zhang's
Horizontal	0.67	0.82	1.04	0.76	0.41
Vertical	89.23	88.64	88.14	88.96	89.67

shown in Table 4, which shows that ICP and OVP exhibited satisfactory reconstruction results within the acceptable scope.

Finally, we explored the parallelism and orthogonality of the reconstructed lines. First, we fitted the lines of each row and column in Fig. 12 using the Hough transform [40]. We calculated the average angle of any two reconstructed lines in the parallel or orthogonal direction, as shown in Table 5. The angles in the parallel and orthogonal directions between any two reconstructed lines based on ICP were 0.67° and 89.23°, respectively, whereas those in the case of OVP were 0.82° and 88.64°, respectively. The angles by Zhang's method were 0.41° and 89.67°. These values are very close to 0° and 90°, respectively, which are the ideal angles in Euclidean space.

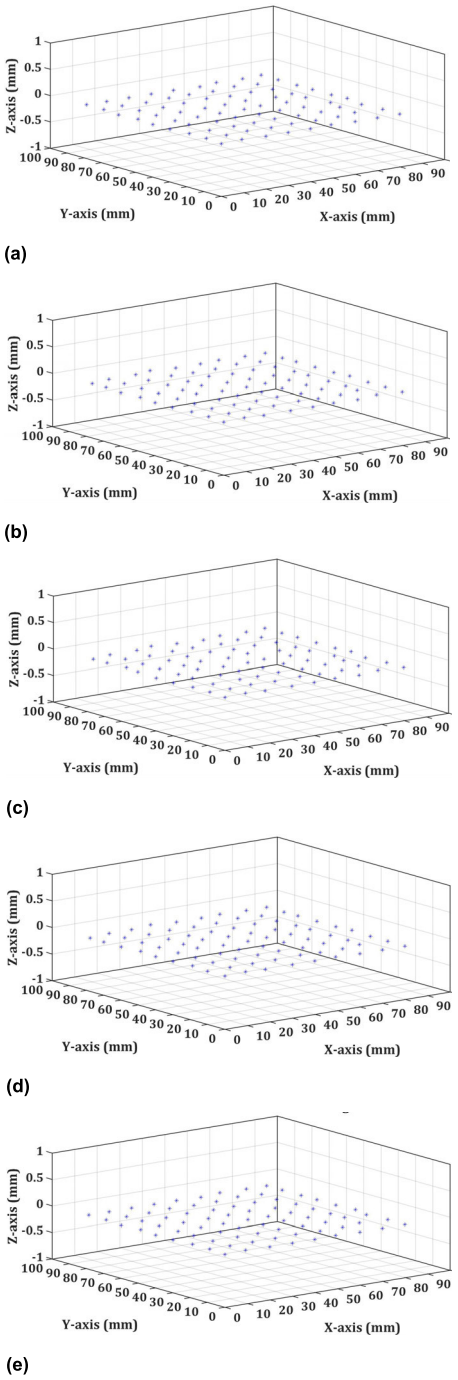

FIGURE 12. Results of 3D reconstruction of angular points using (a) ICP, (b) OVP, (c) TSC, (d) CCT, and (e) Zhang's method.

V. CONCLUSION

In this paper, we proposed a novel, stable, and easy to implement technique for calibrating cameras. This technique requires a 2D calibration pattern, which includes two SSR circles. By analysing the properties of the two SSR circles, we discovered that three lines can be obtained via generalised eigen decomposition. Specifically, one of the lines is a line joining the two circle centres whereas the other two lines are a set of parallel lines perpendicular to it. Based on the

symmetry of the two SSR circles, the other set of parallel lines can be recovered. Subsequently, the imaged circular points and the orthogonal vanishing points can be computed simultaneously. These allow one to determine the constraint on the IAC. Consequently, camera calibration can be completed using at least three images of the two SSR circles. Based on these results, we proposed two calibration methods, which exhibited satisfactory results. Simulations and tests performed using actual images confirmed that the proposed calibration algorithms are robust and effective. Further, by using these methods, one can avoid having to solve quadratic equations, which are sensitive to noise. In addition, in contrast to conventional calibration methods such as Zhang's approach using a planar grid pattern, the proposed methods do not require any high-precision calibration objects or objects with a particular structure and need only two SSR circles with unknown radius and position. Additionally, for Zhang's approach, point matching is vital and needs to be done manually in camera calibration. Moreover, based on the proposed method the camera can be fully linearly calibrated using only generalised eigen decomposition without having to make any assumptions, such as zero skew or a unitary aspect ratio.

As is the case for most calibration methods that use circles, we have not provided a solution for the distortion coefficients. It is difficult to solve lens distortion compared with the chessboard because the correspondence between the apparent contour point and its projection is undetermined. Furthermore, the calibration process will fail in some critical cases. First, when the line connecting the images of the two circle centres passes through or is close to the principal point, the calibration results are poor, because the vanishing point estimated from a set of parallel lines is close to the infinity point on the image plane. Second, when the camera is located at some extreme angles, the SSR circle images cannot be captured. However, in practice, we can easily ensure precise calibration, especially when we have at least three images of two SSR circles. In the future, we will explore an approach for overcoming the above-mentioned difficulties and will focus on developing a unified calibration method based on circles with the same radii, which will include tangent circles, intersecting circles, and enclosing circles.

APPENDIXES

APPENDIX A

Considering two 3×3 symmetric matrices $\mathbf{C}_1$ and $\mathbf{C}_2$, which represent two separate circles. Algebraically, the problem of computing the generalised eigenvectors of matrix pair $\left(\mathbf{C}_1^*, \mathbf{C}_2^*\right)$ is that of determining the eigenvectors of matrix $\mathbf{C}_2\mathbf{C}_1^*$, namely, the generalised eigenvalue decomposition of two circles $\mathbf{C}_1$ and $\mathbf{C}_2$:

$$\mathbf{C}_1^*\mathbf{L} = \beta\mathbf{C}_2^*\mathbf{L}, \tag{27}$$

or

$$\left(\mathbf{C}_1^* - \beta\mathbf{C}_2^*\right)\mathbf{L} = \mathbf{0}_{3\times 3}, \tag{28}$$

or

$$\left(\mathbf{C}_2\mathbf{C}_1^* - \beta\mathbf{I}\right)\mathbf{L} = \mathbf{0}_{3\times 3}, \tag{29}$$

where $\mathbf{I}$ is an identity matrix. Equations (8) and (28) suggest that the generalised eigenvector, $\mathbf{L}$, of $\left(\mathbf{C}_1^*, \mathbf{C}_2^*\right)$ is the null space of circle family $\mathbf{C}^*(\beta)$ consisting of the base circles, $\mathbf{C}_1^*$ and $\mathbf{C}_2^*$. On substituting (28) into (9), we get :

$$\left(\mathbf{C}_1^* - \beta\mathbf{C}_2^*\right)\mathbf{L} = \mathbf{P}\mathbf{Q}^{\mathrm{T}}\mathbf{L} + \mathbf{Q}\mathbf{P}^{\mathrm{T}}\mathbf{L} = \mathbf{0}_{3\times 3}. \tag{30}$$

Because $(\mathbf{P}_i, \mathbf{Q}_i)$ are the degenerate point-pairs of circle family $\mathbf{C}^*(\beta)$, as shown in Fig. 2, the generalised eigenvector, $\mathbf{L}_i$, with eigenvalues $\lambda_i (i = 1, 2, 3)$ comprises the intersection points, $\mathbf{P}_i$ and $\mathbf{Q}_i$, of the common tangent of $\mathbf{C}_1$ and $\mathbf{C}_2$:

$$\lambda_i\mathbf{L}_i = \mathbf{P}_i \times \mathbf{Q}_i, \tag{31}$$

where λ_i is a nonzero scale factor.

If there exists a common self-polar triangle between $\mathbf{C}_1$ and $\mathbf{C}_2$, the vertex, $\mathbf{X}$, and the side, $\mathbf{L}$, of the triangle should satisfy the following relationship [33]:

$$\mathbf{X} = \mathbf{C}_1^*\mathbf{L}, \tag{32}$$

$$\mathbf{X} = \beta\mathbf{C}_2^*\mathbf{L}. \tag{33}$$

Simultaneously solving (32) and (33) gives the following equation:

$$\mathbf{C}_1^*\mathbf{L} = \mathbf{X} = \beta\mathbf{C}_2^*\mathbf{L}. \tag{34}$$

Equations (27) and (34) suggest that the generalised eigenvector, $\mathbf{L}_i$, of $\left(\mathbf{C}_1^*, \mathbf{C}_2^*\right)$ includes the three sides of the common self-polar triangle of $\mathbf{C}_1$ and $\mathbf{C}_2$.

In Fig. 2, one of the sides, $\mathbf{L}_3$, of the common self-polar triangle is formed by the intersection point, $\mathbf{P}_3$, of the internal common tangent and the intersection point, $\mathbf{Q}_3$, of the external common tangent. Hence, $\mathbf{L}_3$ is the line passing through the centres of two circles [34]. Because the common pole of $\mathbf{L}_1$ with respect to $\mathbf{C}_1$ and $\mathbf{C}_2$ is also the intersection point, $\mathbf{E}_2$, of $\mathbf{L}_2$ and $\mathbf{L}_3$, according to the polarity principle [31], line $\mathbf{L}_1$ also passes through the common pole of $\mathbf{L}_3$ with respect to $\mathbf{C}_1$ and $\mathbf{C}_2$, namely, an infinity point, $\mathbf{V}_{1\infty}$, on plane $\mathbf{O}_w X_w Y_w$. Similarly, $\mathbf{V}_{1\infty}$ is also on $\mathbf{L}_2$.

Given that one of the intersection points, $\mathbf{D}$ of line $\mathbf{L}_3$ and circle $\mathbf{C}_1$, and the tangent $\mathbf{L}_\mathrm{d}$ at that point are shown in Fig. 2. Based on the properties of circles, because $\mathbf{L}_3$ is the diameter of $\mathbf{C}_1$, we have $\mathbf{L}_\mathrm{d} \perp \mathbf{L}_3$. Moreover, $\mathbf{L}_\mathrm{d}$ is also the polar of $\mathbf{D}$ with respect to $\mathbf{C}_1$. Therefore, $\mathbf{L}_\mathrm{d}$ passes through $\mathbf{V}_{1\infty}$. Moreover, $\mathbf{L}_1$ and $\mathbf{L}_2$ also pass through $\mathbf{V}_{1\infty}$. As per the properties of projective spaces, $\mathbf{L}_\mathrm{d} \parallel \mathbf{L}_1$, $\mathbf{L}_\mathrm{d} \parallel \mathbf{L}_2$ [31], so $\mathbf{L}_1 \perp \mathbf{L}_3$, $\mathbf{L}_2 \perp \mathbf{L}_3$.

APPENDIX B

As shown in Fig. 3, if there exist two SSR circles $\mathbf{C}_1$ and $\mathbf{C}_2$ on the support plane, on the basis of Proposition 1, the three sides $\mathbf{L}_i (i = 1, 2, 3)$ of the common self-polar triangle of $\mathbf{C}_1$ and $\mathbf{C}_2$ can be obtained from the generalised eigenvalue decomposition of matrix pair $\left(\mathbf{C}_1^*, \mathbf{C}_2^*\right)$. Because two lines,

$\mathbf{L}_1$ and $\mathbf{L}_2$, are parallel to each other and perpendicular to the remaining line, $\mathbf{L}_3$, $\mathbf{L}_1$ and $\mathbf{L}_2$ intersect at infinity point $\mathbf{V}_{1\infty}$:

$$\lambda_{V1}\mathbf{V}_{1\infty} = \mathbf{L}_1 \times \mathbf{L}_2, \tag{35}$$

where λ_{V1} is a nonzero scale factor, and $\times$ denotes the outer product.

It can be seen from Fig. 3 that $\mathbf{L}_1$ exhibits real intersection points $\mathbf{M}_1$ and $\mathbf{M}_2$ with respect to $\mathbf{C}_1$ and only complex intersection points with respect to $\mathbf{C}_2$. Similarly, $\mathbf{L}_2$ exhibits real intersection points $\mathbf{N}_1$ and $\mathbf{N}_2$ with respect to $\mathbf{C}_2$ and only complex intersection points with respect to $\mathbf{C}_1$. Based on the definition of intersecting points, these points, namely, $\mathbf{M}_1, \mathbf{M}_2, \mathbf{N}_1, \mathbf{N}_2$, could be determined using the following equations:

$$\begin{cases} \mathbf{L}_1^{\mathrm{T}} x = 0 \\ x^{\mathrm{T}}\mathbf{C}_1 x = 0, \end{cases} \tag{36}$$

$$\begin{cases} \mathbf{L}_2^{\mathrm{T}} x = 0 \\ x^{\mathrm{T}}\mathbf{C}_2 x = 0. \end{cases} \tag{37}$$

The geometric properties of two SSR circles imply that there is an isosceles triangle $\Delta\mathbf{O}_2\mathbf{N}_1\mathbf{N}_2$. Furthermore, it is not difficult to prove that line $\mathbf{U}_1$, which consists of points $\mathbf{E}_1$ and $\mathbf{N}_1$, is parallel to line $\mathbf{V}_1$, which consists of points $\mathbf{E}_2$ and $\mathbf{M}_2$. Similarly, line $\mathbf{U}_2$ passing through two points, $\mathbf{E}_2$ and $\mathbf{M}_1$, is parallel to line $\mathbf{V}_2$ passing through two points, $\mathbf{E}_1$ and $\mathbf{N}_2$.

Based on the property of invariance for projective projections, the generalised eigenvectors of $\left(\mathbf{C}_1^*, \mathbf{C}_2^*\right)$ would be preserved under the projective transformation from $\mathbf{C}_2\mathbf{C}_1^*$ to $\mathbf{H}^{\mathrm{T}}\mathbf{C}_2\mathbf{C}_1^*\mathbf{H}^{-\mathrm{T}}$. As shown in Fig. 4, there exist two conics, $\mathbf{c}_1$ and $\mathbf{c}_2$, on the image plane, π, representing the images of the two SSR circles. In this case, the generalised eigenvector of $\left(\mathbf{c}_1^*, \mathbf{c}_2^*\right)$ corresponds to three lines, namely, $\mathbf{l}_1, \mathbf{l}_2, \mathbf{l}_3$. Let $\mathbf{l}_1$ intersect $\mathbf{c}_1$ at two points, $\mathbf{m}_1$ and $\mathbf{m}_2$. Further, let it also intersect $\mathbf{l}_3$ at point $\mathbf{e}_1$. Similarly, let $\mathbf{l}_2$ intersect $\mathbf{c}_2$ at two points, $\mathbf{n}_1$ and $\mathbf{n}_2$. Further, let it also intersect $\mathbf{l}_3$ at point $\mathbf{e}_2$. From the above discussion, vanishing point $\mathbf{v}_{1\infty}$ lies on $\mathbf{l}_1$ and $\mathbf{l}_2$:

$$\lambda_{v1}\mathbf{v}_{1\infty} = \mathbf{l}_1 \times \mathbf{l}_2. \tag{38}$$

Line $\mathbf{u}_1$ is formed by connecting $\mathbf{e}_1$ and $\mathbf{n}_1$, while line $\mathbf{v}_1$ is formed by connecting $\mathbf{e}_2$ and $\mathbf{m}_2$. Furthermore, the vanishing point, $\mathbf{v}_{4\infty}$, on $\mathbf{u}_1$ and $\mathbf{v}_1$ can be obtained as follows:

$$\lambda_{v4}\mathbf{v}_{4\infty} = \mathbf{u}_1 \times \mathbf{v}_1, \tag{39}$$

where λ_{v4} is a nonzero scale factor.

Hence, line $\mathbf{u}_2$, which consists of $\mathbf{m}_1$ and line $\mathbf{v}_2$, which consists of $\mathbf{e}_1$ and $\mathbf{n}_2$ intersect at the vanishing point, $\mathbf{v}_{3\infty}$,

$$\lambda_{v3}\mathbf{v}_{3\infty} = \mathbf{u}_2 \times \mathbf{v}_2, \tag{40}$$

where λ_{v3} is a nonzero scale factor.

Then, the vanishing line, $\mathbf{l}_\infty$, can be determined from $\mathbf{v}_{1\infty}$ and $\mathbf{v}_{3\infty}$:

$$\lambda_l\mathbf{l}_\infty = \mathbf{v}_{1\infty} \times \mathbf{v}_{3\infty}, \tag{41}$$

where λ_l is a nonzero scale factor.

REFERENCES

[1] S. Zhang, B. Li, F. Ren, and R. Dong, "High-precision measurement of binocular telecentric vision system with novel calibration and matching methods," *IEEE Access*, vol. 7, pp. 54682–54692, 2019, doi: 10.1109/access.2019.2913181.

[2] M.-C. Kang, C.-H. Yoo, K.-H. Uhm, D.-H. Lee, and S.-J. Ko, "A robust extrinsic calibration method for non-contact gaze tracking in the 3-D space," *IEEE Access*, vol. 6, pp. 48840–48849, 2018, doi: 10.1109/access.2018.2867235.

[3] T. Pribanić, T. Petković, and M. Đonlić, "3D registration based on the direction sensor measurements," *Pattern Recognit.*, vol. 88, pp. 532–546, Apr. 2019, doi: 10.1016/j.patcog.2018.12.008.

[4] M. Wei, Q. Yan, F. Luo, C. Song, and C. Xiao, "Joint bilateral propagation upsampling for unstructured multi-view stereo," *Vis. Comput.*, vol. 35, nos. 6–8, pp. 797–809, Jun. 2019, doi: 10.1007/s00371-019-01688-5.

[5] Y. Fu, Q. Yan, L. Yang, J. Liao, and C. Xiao, "Texture mapping for 3D reconstruction with RGB-D sensor," in *Proc. IEEE/CVF Conf. Comput. Vis. Pattern Recognit.*, vol. 1, Jun. 2018, pp. 4645–4653, doi: 10.1109/cvpr.2018.00488.

[6] Y. Ma, Y. Wang, X. Mei, C. Liu, X. Dai, F. Fan, and J. Huang, "Visible/infrared combined 3D reconstruction scheme based on nonrigid registration of multi-modality images with mixed features," *IEEE Access*, vol. 7, pp. 19199–19211, 2019, doi: 10.1109/access.2019.2895905.

[7] J. Zhang, H. Yu, H. Deng, Z. Chai, M. Ma, and X. Zhong, "A robust and rapid camera calibration method by one captured image," *IEEE Trans. Instrum. Meas.*, vol. 68, no. 10, pp. 4112–4121, Oct. 2019, doi: 10.1109/tim.2018.2884583.

[8] Y. Zhao, Y. Li, and B. Zheng, "Calibrating a paracatadioptric camera by the property of the polar of a point at infinity with respect to a circle," *Appl. Opt.*, vol. 57, no. 15, pp. 4345–4352, May 2018, doi: 10.1364/ao.57.004345.

[9] W. Liu, S. Wu, X. Wu, and H. Zhao, "Calibration method based on the image of the absolute quadratic curve," *IEEE Access*, vol. 7, pp. 29856–29868, 2019, doi: 10.1109/access.2019.2893660.

[10] R. I. Hartley, "An algorithm for self-calibration from several views," in *Proc. IEEE Int. Conf. Comput. Vis. Pattern Recognit.*, vol. 1, Jun. 1994, pp. 908–912, doi: 10.1109/CVPR.1994.323923.

[11] T. Soboda and T. Pajdla, "Epipolar geometry for central catadioptric cameras," *Int. J. Comput. Vis.*, vol. 49, no. 1, pp. 23–27, Jan. 2002, doi: 10.1023/A:1019869530073.

[12] X. Ying and H. Zha, "Geometric interpretations of the relation between the image of the absolute conic and sphere images," *IEEE Trans. Pattern Anal. Mach. Intell.*, vol. 28, no. 12, pp. 2031–2036, Dec. 2006, doi: 10.1109/tpami.2006.245.

[13] K.-Y.-K. Wong, G. Zhang, and Z. Chen, "A stratified approach for camera calibration using spheres," *IEEE Trans. Image Process.*, vol. 20, no. 2, pp. 305–316, Feb. 2011, doi: 10.1109/tip.2010.2063035.

[14] X. Ying and H. Zha, "Identical projective geometric properties of central catadioptric line images and sphere images with applications to calibration," *Int. J. Comput. Vis.*, vol. 78, no. 1, pp. 89–105, Jun. 2008, doi: 10.1007/s11263-007-0082-8.

[15] J. Yu and F. Da, "Bi-tangent line based approach for multi-camera calibration using spheres," *J. Opt. Soc. Amer. A, Opt. Image Sci.*, vol. 35, no. 2, pp. 221–229, Feb. 2018, doi: 10.1364/josaa.35.000221.

[16] Z. Liu, Q. Wu, S. Wu, and X. Pan, "Flexible and accurate camera calibration using grid spherical images," *Opt. Express*, vol. 25, no. 13, pp. 15269–15285, Jun. 2017, doi: 10.1364/oe.25.015269.

[17] H. F. Huang, H. Zhang, and Y. M. Cheung, "Camera calibration based on the common self-polar triangle of sphere images," in *Proc. 12th Asian Conf. Comput. Vis.*, vol. I, pp. 19–29, Jun. 2014, doi: 10.1007/978-3-319-16808-1_2.

[18] H. Zhang, K.-Y.-K. Wong, and G. Zhang, "Camera calibration from images of spheres," *IEEE Trans. Pattern Anal. Mach. Intell.*, vol. 29, no. 3, pp. 499–502, Mar. 2007, doi: 10.1109/tpami.2007.45.

[19] J. S. Kim, P. Gurdjos, and I. S. Kweon, "Euclidean structure from confocal conics: Theory and application to camera calibration," in *Proc. IEEE Int. Conf. Comput. Vis. Pattern Recognit.*, vol. 1, Jun. 2006, pp. 1214–1221, doi: 10.1109/CVPR.2006.115.

[20] S. Cai, Z. Zhao, L. Huang, and Y. Liu, "Camera calibration with enclosing ellipses by an extended application of generalized eigenvalue decomposition," *Mach. Vis. Appl.*, vol. 24, no. 3, pp. 513–520, Apr. 2013, doi: 10.1007/s00138-012-0446-0.

[21] X. H. Ying and H. B. Zha, "Camera calibration using principal-axes aligned conics," in *Proc. 8th Asian Conf. Comput. Vis.*, vol. 1, Nov. 2007, pp. 138–148, doi: 10.1007/978-3-540-76386-4_12.
[22] Z. J. Zhao, "Conics with a common axis of symmetry: Properties and applications to camera calibration," in *Proc. 22nd Int. Joint Conf. Artif. Intell.*, vol. 1, Jul. 2011, pp. 2079–2084, doi: 10.5591/978-1-57735-516-8/IJCAI11-347.
[23] X. Ying and H. Zha, "Camera calibration from a circle and a coplanar point at infinity with applications to sports scenes analyses," in *Proc. IEEE/RSJ Int. Conf. Intell. Robots Syst.*, vol. 1, Oct. 2007, pp. 226–231, doi: 10.1109/iros.2007.4399329.
[24] P. Gurdjos, P. Sturm, and Y. H. Wu, "Euclidean structure from N>=2 parallel circles: Theory and algorithms," in *Proc. 9th Eur. Conf. Comput. Vis.*, vol. 1, May 2006, pp. 238–252, doi: 10.1007/11744023_19.
[25] Q. Chen, H. Y. Wu, and T. Wada, "Camera calibration with two arbitrary coplanar circles," in *Proc. 8th Eur. Conf. Comput. Vis.*, vol. 3, May 2004, pp. 521–532, doi: 10.1007/978-3-540-24672-5_41.
[26] H. Huang, H. Zhang, and Y.-M. Cheung, "The common self-polar triangle of concentric circles and its application to camera calibration," in *Proc. IEEE Conf. Comput. Vis. Pattern Recognit. (CVPR)*, vol. 1, Jun. 2015, pp. 4065–4072, doi: 10.1109/cvpr.2015.7299033.
[27] Q. Chen and H. Wu, "Recovering projected centers of circle-pairs with common tangents," in *Proc. IEEE Int. Conf. Mechatronics Autom. (ICMA)*, Aug. 2017, pp. 1775–1780, doi: 10.1109/icma.2017.8016086.
[28] H. Huang, H. Zhang, and Y.-M. Cheung, "The common self-polar triangle of separate circles: Properties and applications to camera calibration," in *Proc. IEEE Int. Conf. Image Process. (ICIP)*, Sep. 2016, pp. 1170–1174, doi: 10.1109/icip.2016.7532542.
[29] F. Da, Q. Li, H. Zhang, and X. Fang, "Self-calibration using two same circles," *Opt. Laser Technol.*, vol. 44, no. 6, pp. 1924–1933, Sep. 2012, doi: 10.1016/j.optlastec.2012.02.013.
[30] Y. H. Wu, H. J. Zhu, Z. Y. Hu, and F. C. Wu, "Camera calibration from the quasi-affine invariance of two parallel circles," in *Proc. 8th Eur. Conf. Comput. Vis.*, vol. 1, May 2004, pp. 190–202, doi: 10.1007/978-3-540-24670-1_15.
[31] R. Hartley and A. Zisserman, *Multiple View Geometry in Computer Vision*. Cambridge, U.K.: Cambridge Univ. Press, 2004.
[32] J. G. Semple and G. T. Kneebone, *Algebraic Projective Geometry*. Oxford, U.K.: Clarendon Press, 1999.
[33] F. S. Woods, *Higher Geometry*. Boston, MA, USA: Ginn and Company, 1922.
[34] J. Sun, X. Chen, Z. Gong, Z. Liu, and Y. Zhao, "Accurate camera calibration with distortion models using sphere images," *Opt. Laser Technol.*, vol. 65, pp. 83–87, Jan. 2015, doi: 10.1016/j.optlastec.2014.07.009.
[35] A. W. Fitzgibbon, M. Pilu, and R. B. Fisher, "Direct least squares fitting of ellipses," *IEEE Trans. Pattern Anal. Mach. Intell.*, vol. 21, no. 5, pp. 476–480, May 1999, doi: 10.1109/34.765658.
[36] J. Canny, "A computational approach to edge detection," *IEEE Trans. Pattern Anal. Mach. Intell.*, vol. PAMI-8, no. 6, pp. 678–698, Nov. 1986, doi: 10.1109/TPAMI.1986.4767851.
[37] Z. Zhang, "A flexible new technique for camera calibration," *IEEE Trans. Pattern Anal. Mach. Intell.*, vol. 22, no. 11, pp. 1330–1334, 2000, doi: 10.1109/34.888718.
[38] Z. Zhang, "Motion and structure from two perspective views: From essential parameters to Euclidean motion through the fundamental matrix," *J. Opt. Soc. Amer. A, Opt. Image Sci.*, vol. 14, no. 11, pp. 2938–2950, Nov. 1997, doi: 10.1364/josaa.14.002938.
[39] F. Yang, Y. Zhao, and X. Wang, "Calibration of camera intrinsic parameters based on the properties of the polar of circular points," *Appl. Opt.*, vol. 58, no. 22, p. 5901, Aug. 2019, doi: 10.1364/ao.58.005901.
[40] J. Illingworth and J. Kittler, "A survey of the Hough transform," *Comput. Vis., Graph., Image Process.*, vol. 44, no. 1, pp. 87–116, Oct. 1988, doi: 10.1016/S0734-189X(88)80033-1.

FENGLI YANG received the B.S. degree in information and computing science from Yunnan University, Kunming, China, in 2012, and the M.S. degree in operations research and cybernetics from Yunnan University, Kunming, China, in 2017, where he is currently pursuing the Ph.D. degree in computational mathematics. His research interests include 3D stereo measurements, non-contact measurement systems, camera calibration, and applied mathematics.

YUE ZHAO received the B.S. degree in mechanical and electrical engineering from the University of Science and Technology of Tianjin, China, in 1988, and the M.S. degree in automation from Tongji University, Shanghai, China, in l991. He is currently an Associate with the School of Mathematics and Statistics, Yunnan University, China. His main research interests are in the areas of computer vision and computer graphics, which include camera calibration, 3D reconstruction, active vision, geometric invariance and application, 3D vision, and image-based modeling and rendering. He is particularly interested in the development and use of system methodologies and tools to support managerial and learning activities in the above-mentioned areas. His recent research workes focus on computer applications in the fields of catadioptric imaging, robot navigation, and cameras with large fields of view.

XUECHUN WANG received the B.S. degree in information and computing science and the M.S. degree in computational mathematics from Yunnan University, Kunming, China, in 2012 and 2017, respectively, where she is currently pursuing the Ph.D. degree in computational mathematics. Her research interests include optimization and automation of manufacturing processes, computational methods of optimization and error correction, modeling and calibration of coordinate measuring systems, and applied mathematics.